Received February 1999
Revised September 1999
Accepted November 1999

Numerical simulation of a methane/air radiating turbulent diffusion flame

D. Morvan
IRPHE UMR CNRS, Technopôle de Château Gombert, Marseille, France, and
B. Porterie, J.C. Loraud and M. Larini
IUSTI UMR CNRS, Technopôle de Château Gombert, Marseille, France

Keywords *Combustion, Numerical simulation, Turbulence*

Abstract *Reports numerical simulations of an unconfined methane-air turbulent diffusion flame expanding from a porous burner. Turbulent combustion is simulated using the eddy dissipation concept (EDC) which supposes that the reaction rate is controlled by the turbulent structures which enhance the mixing of fuel and oxidant. Two statistical k-ϵ turbulence models have been tested: a standard high Reynolds number (HRN) and a more recent model based on the renormalization group theory (RNG). Radiation heat transfer and soot formation have been taken into account using P1-approximation and transport submodels which reproduce the main phenomena encountered during soot production (nucleation, coagulation, surface growth). The set of coupled transport equations is solved numerically using a high order finite-volume method, the velocity-pressure coupling is treated by a projection technique. The numerical results confirm that 20-25 percent of the combustion heat released is radiated away from the flame. Unsteady and unsymmetrical flame behaviour is observed for small Froude numbers which results from the development of Rayleigh-Taylor like instabilities outside the flame surface. For higher Froude numbers the steady-state and symmetrical nature of the solution is recovered.*

1. Introduction

The progress made in the modelling of turbulent combustion today allows pool fires which develop in an industrial or natural environment to be simulated more realistically. Field models represent a promising way to improve our knowledge of fundamental physical mechanisms associated with fire spread. They should provide a better understanding of the interaction between gas flow dynamics (turbulence, hydrodynamics instabilities), heat flow (by convection, diffusion and radiation), and chemical kinetics (reaction rate, chemical species mixing) (Cox, 1995). Due to the high fluctuation levels observed in turbulent flames, classical moments closure methods generally used in turbulent flow modelling cannot be used for the calculation of

International Journal of Numerical Methods for Heat & Fluid Flow, Vol. 10 No. 2, 2000, pp. 196-227.

The European Economic Commission is gratefully acknowledged for providing partial funding for this research in the frame of the EFASITOS project.

chemical species in turbulent combustion. Various models generally based on physical considerations have been developed to assess multiple interactions between the turbulent structures and the flame dynamics. For infinite fast chemistry, the combustion is controlled by the fuel-oxydant mixing time. In this case the reaction rate can be assessed from a characteristic turbulent time scale (deduced from turbulent kinetic energy and its dissipation rate) and the fluctuation of the fuel mass fraction mixture (eddy break up model for premixed flames) or the average mass fraction of the more deficient chemical species (eddy dissipation concept for diffusion flames). Another approach is based on the use of an assumed shape probability density function (Pdf) which allows finite rate chemical kinetics (Borghi, 1988; Jones and Whitelaw, 1982; Candel *et al.,* 1996; Bray, 1996). In this case the average mass fractions of chemical species are calculated from simple quadrature between instantaneous mass fractions of chemical species expressed as a function of the instantaneous mixture fraction and the Pdf generally evaluated from the average mixture fraction and its fluctuation (Borghi, 1988; Libby and Williams, 1993).

Diffusion flames produced from hydrocarbon combustion are generally very luminous. This luminous emission results from the radiation of soot particles in the flame. The resulting mixture of gaseous reaction products and soot particles can be represented as a gray medium characterized by an absorption coefficient which depends on the combustion product mole fraction, gas temperature and soot volume fraction (Kaplan *et al.,* 1996).

In the present paper, we propose to study numerically the problem of the evolution of a turbulent diffusion flame which develops from the injection of fuel through a porous burner in a free domain initially at rest. Various fuel injection rates have been tested to study the resulting flow pattern and the transition between pool fire and jet flame regimes. The effects of radiation heat transfer and turbulence modelling on the dynamic and thermal fields have also been analysed.

2. Mathematical formulation

Field modelling of fires is based on the resolution of conservation equations (mass, momentum, energy). The buoyancy flow generated by the expansion of hot gas above the flaming zone is great enough to assume that the flow regime can be locally turbulent. To simplify the mathematical formulation of this turbulent flow, a density weighted mean value (or Favre mean value) is used to separate the mean flow and the fluctuations (Cox, 1995). In practice, turbulent diffusion flames such as those studied in the present paper are dominated by buoyancy effects which induce the formation of large scale structures in the plume. To follow these large scale structures above the flame we have adopted an unsteady statistical representation assuming that the time averaging is performed over a long enough period to eliminate fluctuating motions, but shorter than the characteristic time scale for the

coherent structures (Cox, 1995). This approach is sometimes called very large eddy simulation (VLES) or coherent structures modelling (CSM) (Gatski *et al.,* 1996). The turbulent fluxes which appear in the average conservation equations are approximated using the eddy viscosity concept and gradient diffusion hypothesis. Assuming that thermal and species diffusivities are equal (unit Lewis number assumption for equidiffusive flames), the mass, momentum, energy and chemical species conservation equations can be written as follows:

$$\frac{\partial \bar{\rho}}{\partial t} + \frac{d}{\partial x_j}\bar{\rho}\tilde{u_j} = 0 \tag{1}$$

$$\frac{\partial}{\partial t}(\bar{\rho}\tilde{u_i}) + \frac{\partial}{\partial x_j}(\bar{\rho}\tilde{u_j}\tilde{u_i}) = \frac{\partial \overline{\sigma_{ij}}}{\partial x_j} - \frac{\partial \overline{\rho u_j'' u_i''}}{\partial x_j} + \bar{\rho} g_i \tag{2}$$

$$\frac{\partial}{\partial t}\left(\bar{\rho}\tilde{h}\right) + \frac{\partial}{\partial x_j}\left(\bar{\rho}\tilde{u_j}\tilde{h}\right) = \frac{\partial}{\partial x_j}\left(\frac{\bar{\mu}}{P_r}\frac{\partial \tilde{h}}{\partial x_j}\right) + \frac{\partial \bar{p}}{\partial t} - \frac{\partial \overline{\rho} u_j'' h''}{\partial x_j} - \frac{\partial \overline{q_j^R}}{\partial x_j} \tag{3}$$

$$\frac{\partial}{\partial t}\left(\bar{\rho}\widetilde{Y_\alpha}\right) + \frac{\partial}{\partial x_j}\left(\bar{\rho}\tilde{u_j}\widetilde{Y_\alpha}\right) = \frac{\partial}{\partial x_j}\left(\frac{\bar{\mu}}{S_c}\frac{\partial \tilde{Y}_\alpha}{\partial x_j}\right) - \frac{\partial \overline{\rho u_j'' Y_\alpha''}}{\partial x_j} + \overline{\dot{\omega}_\alpha} \tag{4}$$

where P_r and S_c are the Prandtl and Schmidt numbers respectively. Here, ρ, p, u_i, h, σ_{ij}, μ, Y_α, $\dot{\omega}_\alpha$, g_i, q_j^R are the density, pressure, velocity component in the x_i direction, enthalpy, stress tensor, viscosity, mass fraction and mass production rate of species α, gravity acceleration component in the x_i direction, and radiative heat flux. The superscripts $\bar{(\ )}$, $\tilde{(\ )}$, and $(\ )''$ denote the time average, density-weighted Favre average and density-weighted Favre fluctuation. The turbulent fluxes for momentum and scalar quantity transport equations are evaluated using the eddy viscosity concept and gradient diffusion hypothesis:

$$-\overline{\rho u_j'' u_i''} = \mu_t\left[\frac{\partial \tilde{u_i}}{\partial x_j} + \frac{\partial \tilde{u_j}}{\partial x_i}\right] - \frac{2}{3}\left[\mu_t \frac{\partial \tilde{u_k}}{\partial x_k} + \bar{\rho}k\right]\delta_{ij} \tag{5}$$

$$-\overline{\rho u_j'' \phi''} = \frac{\mu_t}{\sigma_\phi}\frac{\partial \tilde{\phi}}{\partial x_j} \tag{6}$$

where the turbulent Prandtl number appropriate to ϕ, σ_ϕ, is taken to be 0.7. The eddy viscosity μ_t is evaluated from the turbulent kinetic energy (k) and its dissipation rate (ϵ).

$$\mu_t = \bar{\rho} C_\mu \frac{k^2}{\epsilon} \tag{7}$$

To assess these two scalar quantities which define the turbulent transport, a k-ϵ model constructed from the renormalization group (RNG) theory has been used (Mohammadi and Pironneau, 1994; Yakhot and Orszag, 1986). The main advantage of this particular approach in comparison with the standard k-ϵ turbulence modelling, is the wide range of validity for the calculation of the eddy viscosity. This turbulence modelling is adapted for both weak and fully developed turbulent flows (Mohammadi and Pironneau, 1994; Yakhot and Orszag, 1986) which typically represents the conditions encountered for turbulent diffusion flames. The turbulent kinetic energy (k) and its dissipation rate (ϵ) are evaluated from two transport equations (Yakhot and Smith, 1992):

$$\frac{\partial}{\partial t}(\bar{\rho}k) + \frac{\partial}{\partial x_j}(\bar{\rho}\tilde{u}_j k) = \frac{\partial}{\partial x_j}\left(\left(\overline{\mu} + \frac{\mu_t}{\sigma_k}\right)\frac{\partial k}{\partial x_j}\right) + P_k + W_k - \bar{\rho}\epsilon \tag{8}$$

$$\frac{\partial}{\partial t}(\bar{\rho}\epsilon) + \frac{\partial}{\partial x_j}(\bar{\rho}\tilde{u}_j \epsilon) = \frac{\partial}{\partial x_j}\left(\left(\overline{\mu} + \frac{\mu_t}{\sigma_\epsilon}\right)\frac{\partial \epsilon}{\partial x_j}\right) + (C_{\epsilon 1} - R)\frac{\epsilon}{k}P_k$$

$$+ C_{\epsilon 3}\frac{\epsilon}{k}W_k - C_{\epsilon 2}\bar{\rho}\frac{\epsilon^2}{k} \tag{9}$$

where P_k and W_k are the shear stress and buoyancy turbulent production terms respectively:

$$P_k = -\overline{\rho u_i'' u_j''}\frac{\partial \tilde{u}_i}{\partial x_j} \quad W_k = -\frac{\mu_t}{\bar{\rho}^2}\frac{\partial \bar{\rho}}{\partial x_j}\frac{\partial \bar{p}}{\partial x_j} \quad R = \frac{\eta(1 - \eta/\eta_0)}{1 + \beta\eta^3} \tag{10}$$

$$\eta = \sqrt{\frac{P_k}{C_\mu \bar{\rho}\epsilon}} \quad \eta_0 = 4.38 \quad \beta = 0.015 \quad C_\mu = 0.0845 \tag{11}$$

$$C_{\epsilon 1} = 1.42 \quad C_{\epsilon 2} = 1.68 \quad C_{\epsilon 3} = 1.5 \quad \sigma_k = 0.7179 \quad \sigma_\epsilon = 1.3 \tag{12}$$

To study the modifications introduced using this turbulence modelling, we have performed another calculation using a classical high Reynolds number (HRN) k-ϵ model where the turbulence variables are evaluated as follows:

$$\frac{\partial}{\partial t}(\bar{\rho}k) + \frac{\partial}{\partial x_j}(\bar{\rho}\widetilde{u}_j k) = \frac{\partial}{\partial x_j}\left(\left(\overline{\mu} + \frac{\mu_t}{\sigma_k}\right)\frac{\partial k}{\partial x_j}\right) + P_k + W_k - \bar{\rho}\epsilon \tag{13}$$

$$\frac{\partial}{\partial t}(\bar{\rho}\epsilon) + \frac{\partial}{\partial x_j}(\bar{\rho}\widetilde{u}_j \epsilon) = \frac{\partial}{\partial x_j}\left(\left(\overline{\mu} + \frac{\mu_t}{\sigma_\epsilon}\right)\frac{\partial \epsilon}{\partial x_j}\right) + C_{\epsilon 1}\frac{\epsilon}{k}(P_k + W_k)$$

$$- C_{\epsilon 2}\bar{\rho}\frac{\epsilon^2}{k} \tag{14}$$

The values for the empirical constants are (Jones and Whitelaw, 1982):

$$C_\mu = 0.09 \quad C_{\epsilon 1} = 1.45 \quad C_{\epsilon 2} = 1.92 \quad \sigma_k = 1.0, \quad \sigma_\epsilon = 1.3 \tag{15}$$

Compared with the standard model, the RNG turbulence model introduces a further term R in the transport equation for ϵ which introduces a spatially and a temporally varying balance between the production and dissipation terms. In regions of low turbulence level the RNG eddy viscosity has a cut-off, below which the eddy viscosity is zero (Yakhot and Orszag, 1986; Orszag, 1996) The radiation heat transfer is treated using the P_1-approximation model (Fusegi and Farouk, 1989; Siegel and Howell, 1992), which assumes the gas mixture to be a gray medium with a mean absorption coefficient defined from the mole fraction of combustion products, soot volume fraction and mean temperature (Kaplan *et al.*, 1996). In this case the radiation heat transfer equation and the heat lost by radiation can be written as (the contribution due to temperature fluctuations is neglected):

$$\frac{\partial}{\partial x_j}\left(\frac{1}{3a_R}\frac{\partial J}{\partial x_j}\right) = a_P\left[J - 4n^2\sigma\widetilde{T}^4\right] \tag{16}$$

$$-\frac{\partial \overline{q_j^R}}{\partial x_j} = a_P\left[J - 4n^2\sigma\widetilde{T}^4\right] \tag{17}$$

where J, a_R, a_P, σ, T and n represent the irradiance, Rosseland and Planck absorption coefficients, Stefan-Boltzmann constant, average temperature and refracting index of the semi-transparent medium respectively. The average soot number density ($\widetilde{n_d}$) and soot volume fraction ($\widetilde{f_v}$) can be solved from two coupled transport equations including nucleation, coagulation of soot particles and surface growth mechanisms along with also the contribution due to turbulent transport (Kaplan *et al.*, 1996):

$$\frac{\partial \bar{\rho}\widetilde{n_d}}{\partial t} + \frac{\partial}{\partial x_j}(\bar{\rho}\widetilde{u_j}\widetilde{n_d}) = -\bar{\rho}\frac{\partial}{\partial x_j}\left(\widetilde{u_j^{th}}\widetilde{n_d}\right) - \frac{\partial \overline{\rho u_j'' n_d''}}{\partial x_j} + \overline{\rho\dot{\omega}_{n_d}} \tag{18}$$

$$\frac{\partial \bar{\rho}\widetilde{f_v}}{\partial t} + \frac{\partial}{\partial x_j}(\bar{\rho}\widetilde{u_j}\widetilde{f_v}) = -\bar{\rho}\frac{\partial}{\partial x_j}\left(\widetilde{u_j^{th}}\widetilde{f_v}\right) - \frac{\partial \overline{\rho u_j'' f_v''}}{\partial x_j} + \overline{\rho\dot{\omega}_{f_v}} \tag{19}$$

$$\overline{\rho\dot{\omega}_{n_d}} = \underbrace{N_0 C_\alpha \bar{\rho}^3 \widetilde{T}^{1/2}\widetilde{X_{Fu}} e^{-T_\alpha/\widetilde{T}}}_{nucleation} - \underbrace{\bar{\rho}C_\beta \widetilde{T}^{1/2}\frac{\widetilde{n_d}^2}{N_0}}_{coagulation} \tag{20}$$

$$\overline{\rho\dot{\omega}_{f_v}} = \underbrace{\frac{C_\delta C_\alpha}{\rho_{soot}}\bar{\rho}^3 \widetilde{T}^{1/2}\widetilde{X_{Fu}} e^{-T_\alpha/\widetilde{T}}}_{nucleation} + \underbrace{\frac{C_\gamma}{\rho_{soot}^{1/3}}\widetilde{n_d}^{1/3}\widetilde{f_v}^{2/3}\bar{\rho}^2 \widetilde{T}^{1/2}\widetilde{X_{Fu}} e^{-T_\gamma/\widetilde{T}}}_{surface\ growth} \tag{21}$$

where the mean thermophoretic velocity and the absorption coefficient are approximated from the following expressions:

$$\widetilde{u_j^{th}} = -0.54\nu\frac{\partial \ln \widetilde{T}}{\partial x_j} \tag{22}$$

$$a_{CO_2+H_2O} = 0.001\left(\widetilde{X_{CO_2}} + \widetilde{X_{H_2O}}\right) \quad (\mathrm{cm}^{-1}) \tag{23}$$

$$a_{soot} = 18.62\widetilde{f_v}\widetilde{T} \quad (\mathrm{cm}^{-1}) \tag{24}$$

$$a_P = a_{CO_2+H_2O} + a_{soot} \tag{25}$$

The empirical constants which define the soot production rate are:

$$C_\alpha = 6.54\,10^4\ \mathrm{m^3/(kgK^{1/2}s)}, C_{\overline{\beta}} = 1.3\,10^7\ \mathrm{m^3/(K^{1/2}s)},$$
$$C_\gamma = 0.1\ \mathrm{m^3/(kg^{2/3}K^{1/2}s)}, C_\delta = 144\ \mathrm{kg}, T_\alpha = 4.61\,10^4\,K,$$
$$T_\gamma = 1.26\,10^4\,K, \rho_{\mathrm{soot}} = 1,800\ \mathrm{kg/m^3}.$$

Turbulent combustion modelling consists in defining a relationship between the reaction rate, turbulence variables (k, $\epsilon \ldots$) and average or mean square fluctuations of mass fractions (chemical species, mixture fraction). To reduce the number of transport equations needed to evaluate the gas mixture, it is more convenient to introduce the mixture fraction $\widetilde{f}$

$$\widetilde{f} = \frac{\zeta - \zeta_2}{\zeta_1 - \zeta_2} \quad \zeta = \widetilde{Y_{Fu}} - \frac{\widetilde{Y_{Ox}}}{s} \tag{26}$$

where the subscripts 1,2 denote fuel and ambient air conditions, and s refers to the stoichiometric oxidant requirement to burn a unit mass of fuel (for a methane-air diffusion flame $s = 4$).

Combining the transport equations of the fuel and oxidant species and using the equal species diffusivities assumption, the conservation equation for the average mixture fraction can be written:

$$\frac{\partial}{\partial t}(\bar{\rho}\widetilde{f}) + \frac{\partial}{\partial x_j}(\bar{\rho}\widetilde{u_j}\widetilde{f}) = \frac{\partial}{\partial x_j}\left[\left(\frac{\bar{\mu}}{Pr} + \frac{\bar{\mu}_t}{\sigma_f}\right)\frac{\partial \widetilde{f}}{\partial x_j}\right] \tag{27}$$

As previously mentioned, the reaction rate is evaluated using the eddy dissipation concept (EDC) (Magnussen and Hjertager, 1976) which is based on the following assumptions:

(1) the instantaneous chemistry can be considered to be fast compared to the turbulence characteristic time;

(2) the average reaction rate is a function of the fuel-oxidant mixing time which depends on turbulence transport.

Therefore the average fuel mass fraction and the mean reaction rate are evaluated from Magnussen and Hjertager (1976):

$$\frac{\partial}{\partial t}(\bar{\rho}\widetilde{Y_{Fu}}) + \frac{\partial}{\partial x_j}(\bar{\rho}\widetilde{u_j}\widetilde{Y_{Fu}}) = \frac{\partial}{\partial x_j}\left[\left(\frac{\bar{\mu}}{Pr} + \frac{\bar{\mu}_t}{\sigma_f}\right)\frac{\partial \widetilde{Y_{Fu}}}{\partial x_j}\right] + \overline{\dot{\omega}_{Fu}} \tag{28}$$

where the mean fuel consumption rate is evaluated from the turbulence integral time scale and the more deficient chemical species (fuel, oxidant or combustion

products) as follows (Magnussen and Hjertager, 1976):

$$\overline{\dot{\omega}_{fu}} = -A\frac{\epsilon}{k}\bar{\rho}\min\left(\widetilde{Y_{fu}}, \frac{\widetilde{Y_{Ox}}}{s}, \frac{B\widetilde{Y_{Pro}}}{1+s}\right) \tag{29}$$

and the two constants A and B are respectively equal to 4 and 0.5.

3. Numerical method

The conservation equations for mass, momentum, energy and species, along with turbulence and soot transport equations can be written under a generic convection-diffusion transport equation as follows:

$$\frac{\partial}{\partial t}(\rho\psi) + \frac{\partial}{\partial x_j}(\rho u_j \psi) = \frac{\partial}{\partial x_j}\left(\Gamma\frac{\partial \psi}{\partial x_j}\right) + S_\psi \tag{30}$$

where ψ represents a transported variable (h, v_i), Γ is the diffusion coefficient, and S_ψ a source term. Using a second-order backward Euler scheme for the time integration, these transport equations can be integrated over each control volume which forms an approximation of the computational domain (Patankar, 1981). Associated with adequate boundary conditions we obtain an algebraic equation:

$$\left[3(\rho_P\psi_P)^{n+1} - 4(\rho_P\psi_P)^n + (\rho_P\psi_P)^{n-1}\right]\frac{\delta\Omega}{2\delta t} + J_e - J_w + J_n - J_s = S_\psi{}^{n+1}\delta\Omega \tag{31}$$

$$J_i = \left[\rho u_i\psi_i - \Gamma_i\left(\frac{\partial\psi}{\partial x_j}\right)_i\right]^{n+1} \delta_i \quad i = \text{east(e), west(w), north(n), and south(s) nodes} \tag{32}$$

where δt, $\delta\Omega$, u_i and δ_i are respectively the time step, cell volume, normal velocity and transverse grid size at the interface i between two contiguous control volumes; n+1, n, n-1 refer to successive integration times. The evaluation of the interface flux between two adjacent finite volumes (J_i) depends on the choice of the numerical scheme. The diffusion term is generally discretized using the second-order central-difference scheme. The same approach could not be used to calculate convective terms because of the growth of unphysical oscillations and instabilities generated since the cell Peclet number P_Δ ($P_\Delta = |U|\Delta/\Gamma$) is greater than 2 (where $|U|$, Δ refer to the velocity modulus and the mesh size respectively). The alternative solution to avoid this well-known oscillatory behaviour of a central-difference scheme

consists in approximating the convective flux using upwind schemes. It is well established that the introduction of first-order approximations (upwind, power law, hybrid (Patankar, 1981)) allows the construction of very robust non-oscillatory convective schemes but can introduce significant numerical diffusion. In this case the effective diffusion introduced in the discretized transport equations is considerably greater than the real physical value (Leonard and Drummond, 1995). An alternative is to use higher order upwind schemes. A high order upwind scheme can be introduced for incompressible and density variable fluid flows using an ultra-sharp approach (universal limiter for tight resolution and accuracy with a simple high accuracy resolution program (Leonard and Mokhtari, 1990)). This numerical method is based on a high order upwind scheme for the convective terms while applying a universal flux limiter (the downwind weighting factor (DWF)) to eliminate any possibility of overshoot or oscillation sometimes introduced when the monotonicity of the solution is not ensured. Depending on the direction of the convective velocity, three values for the unknown variables (ψ) are defined in more detail, namely the upwind (ψ_U), downwind (ψ_D) and central point (ψ_C) values (see Figure 1). The evaluation of the unknown variable at the interface is:

$$\psi_f = DWF\psi_D + (1 - DWF)\psi_C \tag{33}$$

where DWF is the downwind factor, defined from the following expression:

$$DWF = \frac{\psi_f^{up} - \psi_C}{\psi_D - \psi_C} \tag{34}$$

where ψ_f^{up} represents a high order upwind approximation of the unknown at the interface between two control volumes. It can be evaluated from the third-order QUICK scheme

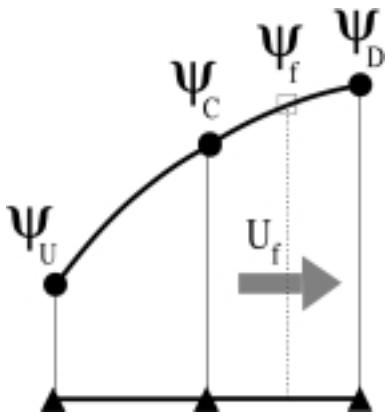

Figure 1.
Definition of upwind (ψ_U), centred (ψ_C), downwind (ψ_D), and interface (ψ_f) variables

$$\psi_f^{up} = \frac{3}{8}\psi_D + \frac{3}{4}\psi_C - \frac{1}{8}\psi_U \tag{35}$$

In non-monotonous situations the use of a high order upwind scheme induces undershoots and overshoots. To eliminate this unacceptable behaviour the DWF must be corrected using a flux limiter strategy (Leonard and Mokhtari, 1990). It is more convenient to summarize the limiter constraints in terms of normalized variable ($\tilde{\psi}$), which is defined as

$$\tilde{\psi} = \frac{\phi - \psi_U}{\psi_D - \psi_U} \tag{36}$$

In the normalized variable diagram (NVD), namely the $(\tilde{\psi_C}, \tilde{\psi_f})$ plane, the DWF can be evaluated from

$$DWF = \frac{\tilde{\psi_f} - \tilde{\psi_C}}{1 - \tilde{\psi_C}} \tag{37}$$

and the flux limiting strategy represented in Figure 2 as the grey region, can be summarized as:

$$\text{if} \quad \widetilde{\psi_C} \leq 0 \quad \text{and} \quad \widetilde{\psi_C} \geq 1 \quad \text{then} \quad \widetilde{\psi_f} = \widetilde{\psi_C} \tag{38}$$

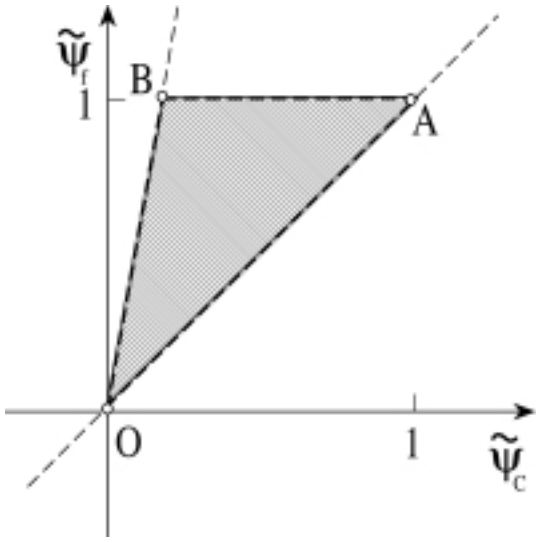

Figure 2.
Universal limiter constraints in the normalized variables diagram (NVD)

$$\text{if} \quad 0 < \widetilde{\psi_C} < 1 \quad \text{then} \quad \widetilde{\psi_f} = \frac{\phi_f^{up} - \phi_U}{\phi_D - \phi_U} \tag{39}$$

$$\widetilde{\psi_f} = \max\left(\widetilde{\psi_f}, \widetilde{\psi_C}\right) \quad \widetilde{\psi_f} = \min\left(\widetilde{\psi}_{\mathrm{f}}, \mathrm{C}\widetilde{\psi_{\mathrm{C}}}\right) \quad \widetilde{\psi}_{\mathrm{f}} = \min\left(\widetilde{\psi}_{\mathrm{f}}, 1\right) \tag{40}$$

For an unsteady problem $C = U_f \delta t / \delta$ (Courant number) (Leonard and Mokhtari, 1990). To reduce the memory size the present problem is solved using a segregated algorithm, the pressure-velocity coupling is treated using a pressure correction or a projection method (Libby and Williams, 1993).

4. Results and discussion

Figure 3 shows a schematic representation of the physical problem of an unconfined turbulent pool fire. The dimensions of the computational domain are $4\mathrm{m} \times 4\mathrm{m}$. Fuel injection is performed through a porous burner (20cm long) located in the middle of the bottom boundary. Neumann conditions are imposed at the free boundaries for all the variables with the exception of pressure which is assumed to be equal to the hydrostatic pressure. At the wall, outside the injection zone, Neumann boundary conditions are assumed for pressure, enthalpy, mixture fraction, and soot quantities. For the turbulence variables the following conditions are imposed (Schiestel, 1993; Zijlema *et al.*, 1995):

$$k_w = 0 \quad \epsilon_w = \frac{{k_\Delta}^{3/2} {C_\mu}^{3/4}}{K\Delta} \tag{41}$$

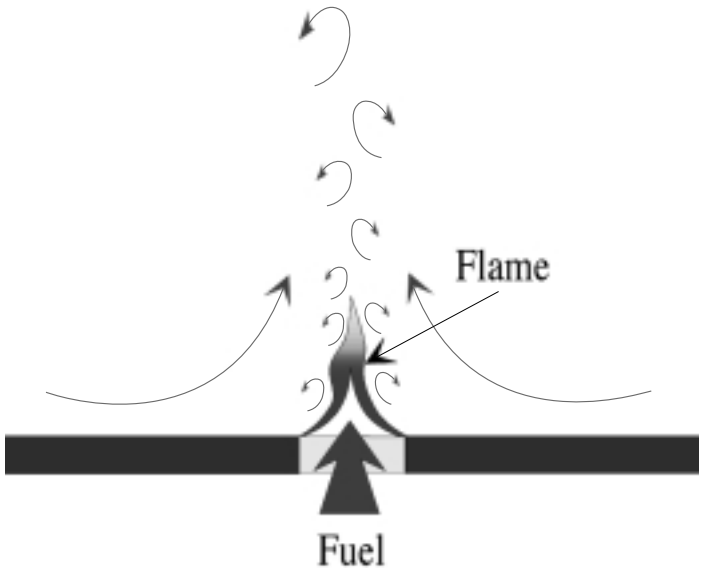

Figure 3.
Development of a turbulent diffusion flame from a porous burner (schematic representation)

where k_Δ represents the turbulent kinetic energy at a finite distance Δ near the wall and K the Von Karman constant ($K = 0.42$). We have tested five values for the fuel injection rates $\rho U_{fuel} = 0.0025$, 0.005, 0.01, 0.05, $0.1 \mathrm{kg/m^2/s}$, adjusted to give heat release rates $P = \rho U_{fuel} \times d \times H_c = 25$, 50, 100, 500 and 1000kW/m, respectively. d and H_c represent the burner diameter and the reaction heat. For methane/air flame $H_c = 5\,10^7 \mathrm{J/kg}$.

In the fuel injection zone, the mixture fraction and fuel mass fraction is equal to unity. Fuel is injected at ambient temperature and low turbulence level (k, $\epsilon = 10^{-6}$). The mesh used for the present calculations consists of 75×80 finite volumes refined horizontally near the bottom wall and vertically along the symmetry axis perpendicular to the burner (Figure 4). Unsteady calculations are carried out using a constant time step $\Delta t = 10^{-2}\mathrm{s}$.

4.1. Influence of turbulence modelling

To study turbulence effects on the flame behaviour, predicted temperature and velocity vector fields obtained using the RNG and HRN k-ϵ turbulence models at $t = 20\mathrm{s}$ are presented in Figures 5 and 6 for an intermediate heat release rate of 100kW/m. The comparative examination of these results reveals significant discrepancies. From predicted results obtained using the RNG model, it is seen that the flame becomes dynamic in nature, with large buoyancy-driven vortices

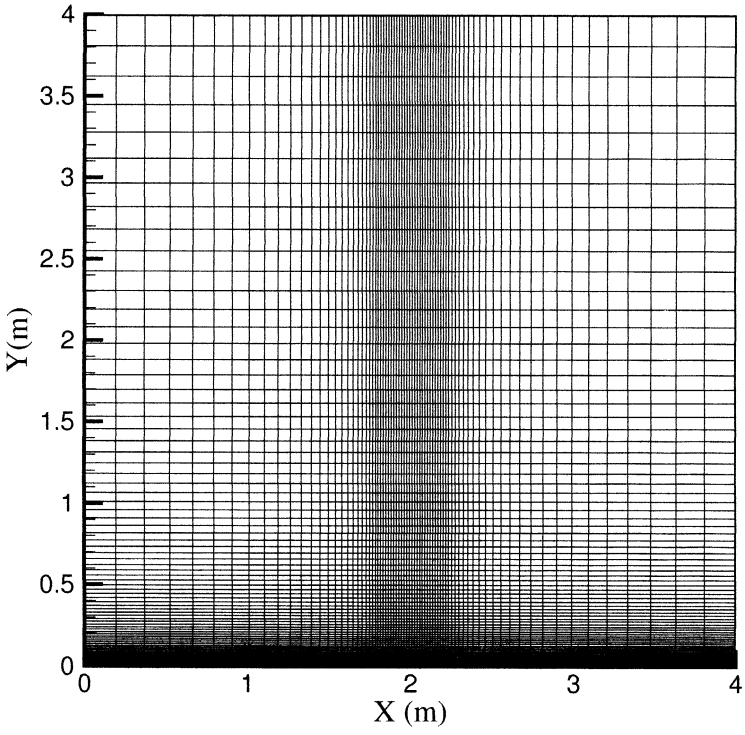

Figure 4.
Computational grid used in the simulations

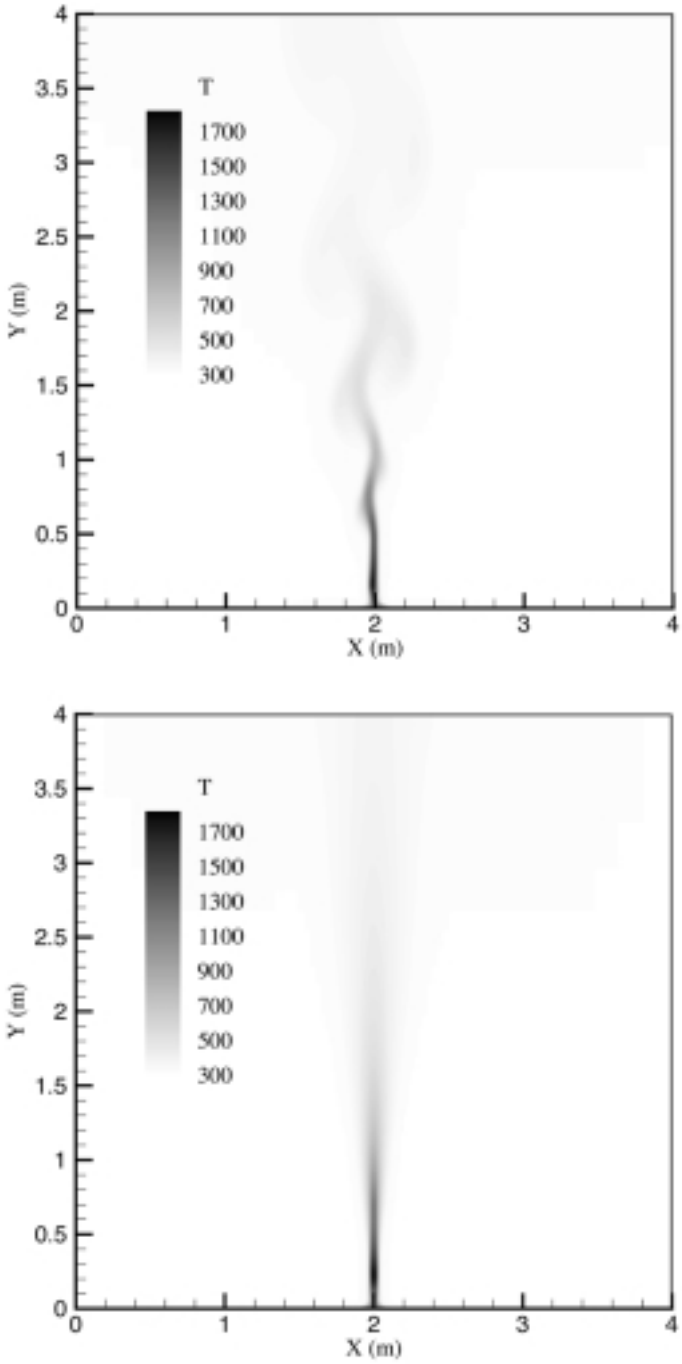

Figure 5.
Methane/air turbulent diffusion flame (P = 100kW/m): temperature field obtained using RNG (top) and HRN (bottom) turbulence models

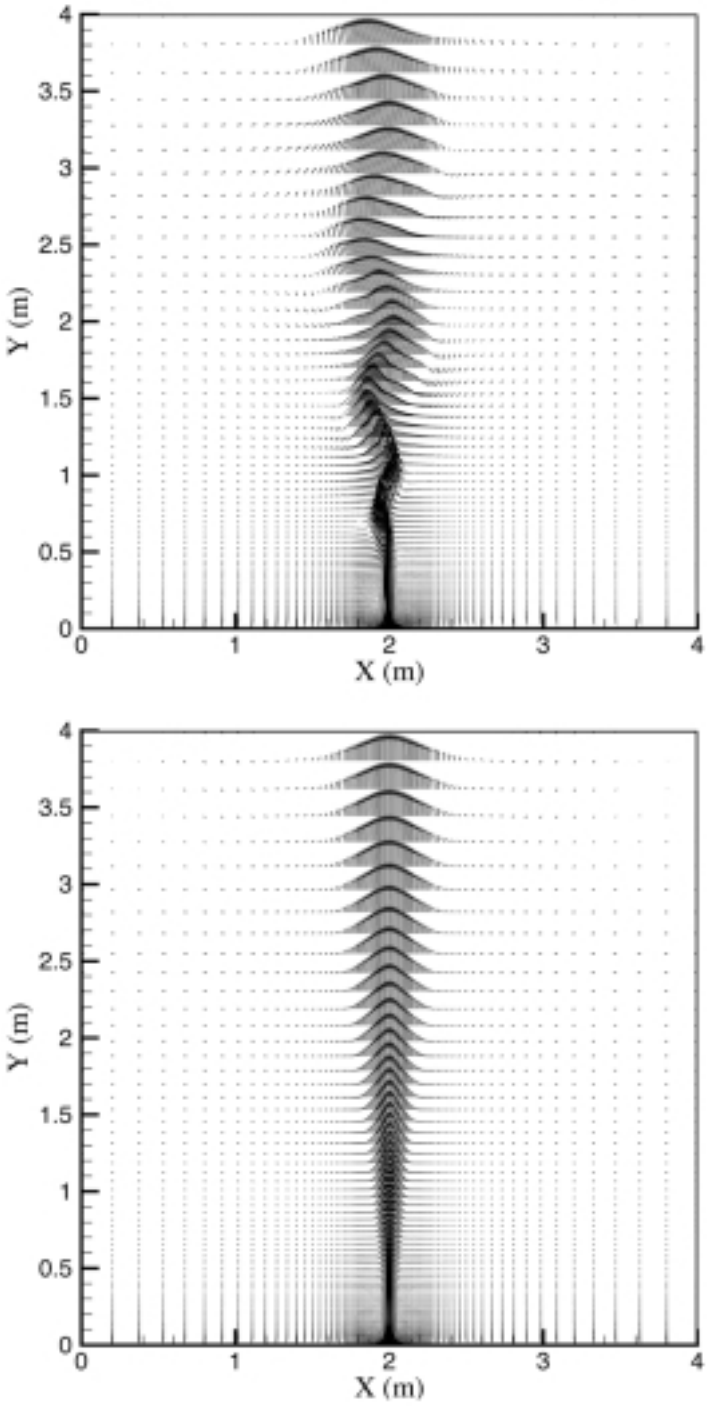

Figure 6.
Methane/air turbulent diffusion flame (P = 100kW/m): velocity vector field obtained using RNG (top) and HRN (bottom) turbulence models (U_{max} = 5.2 and 4.8m/s, respectively)

developing outside the flame surface. Using the HRN model the predicted flow and thermal fields are symmetrical in relation to the burner centerline. This is confirmed by the temperature profiles at different heights $y = 0.01$, 0.05, 0.1, 0.2, 0.5 and 1m above the exit of the burner in Figure 7 where the break in symmetry is clearly seen in the results obtained with the RNG model. The solution obtained using the HRN model is steady while that obtained using the RNG model is unsteady as shown in Figure 8 where the time evolution of the flame height is plotted for both models. These results conform with previous studies which have demonstrated that the overestimation of turbulence kinetic energy engendered by standard k-ϵ model can induce a damping or total disappearance of coherent structures and secondary flows which are generally observed in a large variety of turbulent flows (wakes, jets, ducts). This major weakness in the standard k-ϵ approach can be corrected using non-linear or RNG models which significantly improve the representation of such turbulent flows (Mohammadi and Pironneau, 1994; Speziale, 1987). The unsteady behaviour of pool fires shown in the present calculation conforms with experimental observations (Drysdale, 1985; Cox, 1995).

4.2. Influence of radiation

To illustrate the influence of radiation on flame behaviour, calculations using the RNG model and neglecting radiation effects have been performed for the same conditions (P = 100kW/m). The corresponding temperature field and temperature profiles at different heights are shown in Figure 9. They are to be compared to those plotted in Figures 5 and 7 (upper diagrams). Up to a height $Y = 0.1\mathrm{m}$, the temperature profiles are not significantly affected by radiation while at heights $Y = 0.2$, 0.5 and $1\mathrm{m}$ discrepancies occur. Near the flame tip, radiative heat losses cause the magnitude of the temperature peak to decrease from 2,300K to 1,800K. It can be estimated that from 20 to 25 percent of the heat released is radiated away from the flame. This is in agreement with previous studies (Cox, 1995; Kaplan *et al.,* 1996; Kaplan *et al.*, 1994; Said *et al.,* 1997) of laminar and turbulent sooting flames. These results can in fact be explained from the soot volume fraction profiles (Figure 10) since, below $Y = 0.1\mathrm{m}$, the medium is nearly transparent due to the weak soot concentration in the pre-flame region where the fuel and oxidant are mixed and react. In the post-flame region (Said *et al.*, 1997), namely for $Y \geq 0.2\mathrm{m}$ in Figure 10, the soot volume fraction increases to reach a maximum value of $1.1\ 10^{-6}$ at $Y = 0.5\mathrm{m}$. In this region associated with a large absorption coefficient due to the high soot and combustion product concentration, the radiative heat losses are significant.

4.3. Transient behaviour and fire regimes with heat release rate

The development of the flame in four-second intervals from the beginning of fuel injection to 16s is presented in Figures 11 and 12 for a case with $P = 100\mathrm{kW/m}$. In this transient development, at $t = 4\mathrm{s}$, the occurrence of vortices is observed, shown by the "mushroom" clouds on both sides of the burner axis. These vortices merge and are convected vertically outside the

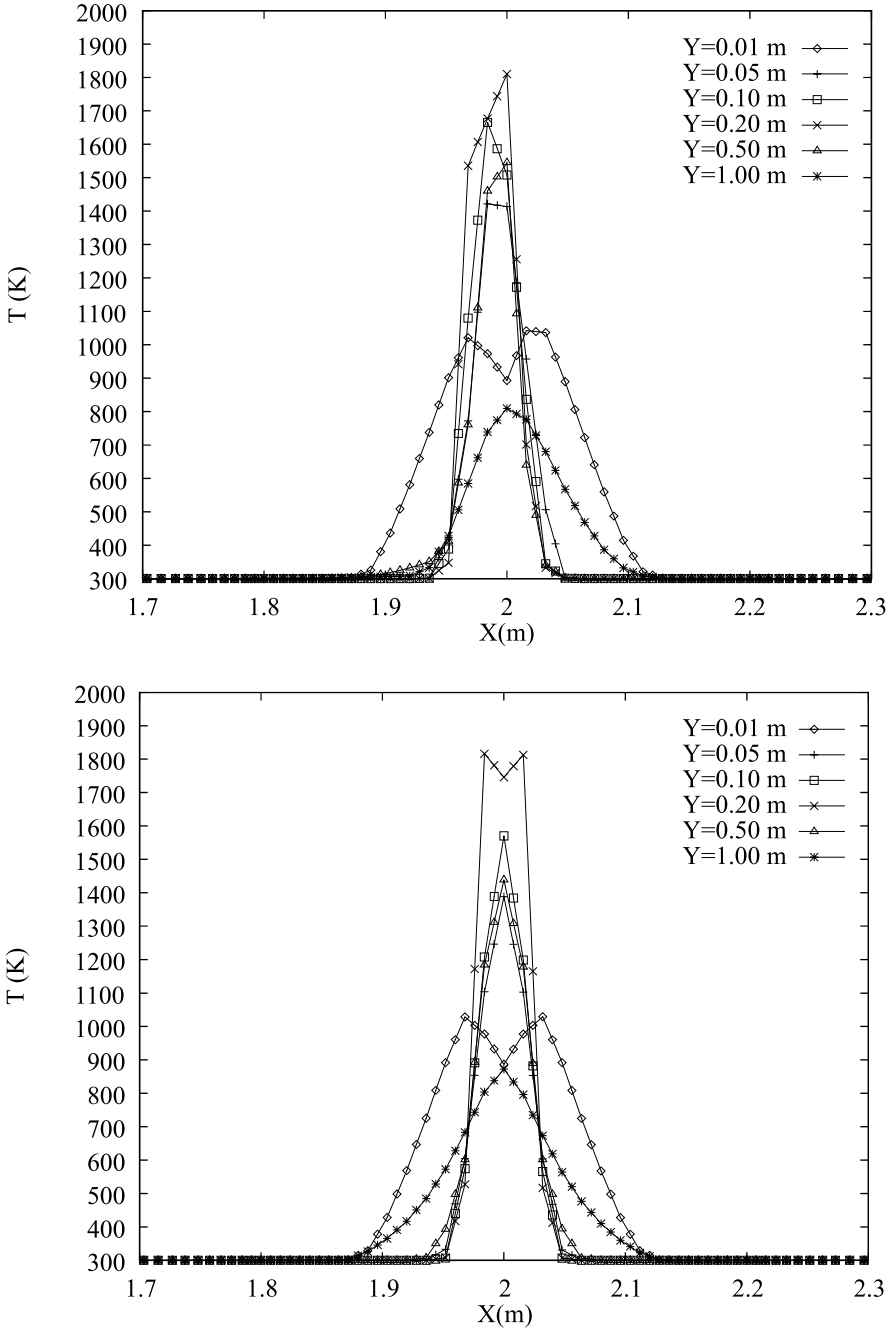

Figure 7.
Methane/air turbulent diffusion flame (P = 100kW/m): temperature profiles obtained using RNG (top) and HRN (bottom) turbulence models

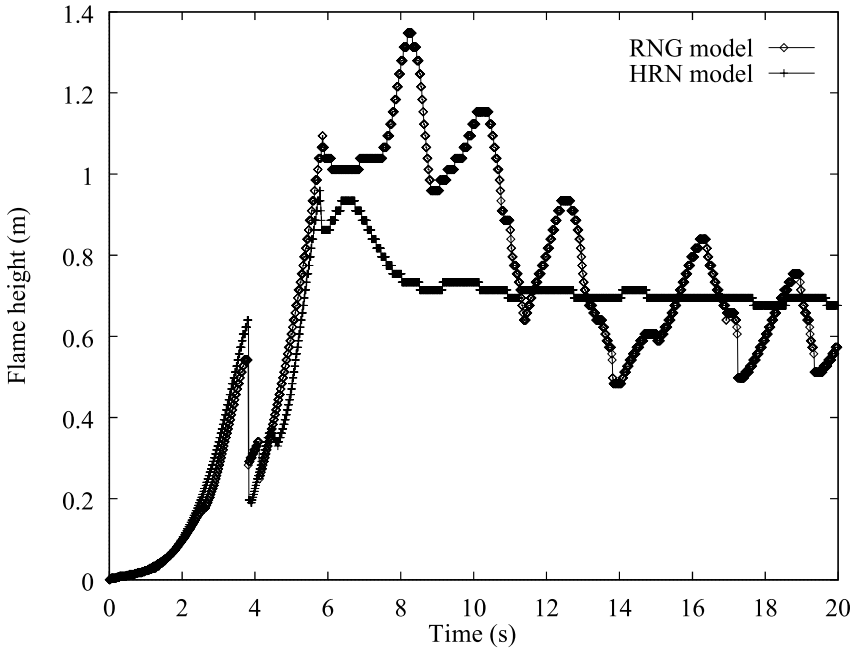

Figure 8.
Flame height as a function of time obtained using RNG and HRN turbulence models

computational domain (Figure 11). From $t = 8$s, Rayleigh-Taylor instabilities which develop on both sides of the burner axis induce alternate vortices which can be visualized by the wavy thermal plume in Figure 12. This unsteady behaviour is in agreement with direct numerical simulations and experimental studies (Davis *et al.*, 1991) carried out for a propane jet flame which have shown the formation of vortices inside and outside the flame surface. Predicted temperature and velocity vector fields are presented in Figures 13, 14, 15 and 16 for cases with a heat release rate which range from 25 to 1,000kW/m. The basic diffusion flame structure can be classified in two regimes from buoyant flame regime (Regime 1) to the jet flame regime (Regime 2) where inertial effects are dominant (Caffrey, 1988). The introduction of a characteristic parameter $Q^\star$ is useful in the discussion of such regimes:

$$Q^\star = \frac{\rho_{fuel}}{\rho_\infty}\frac{\Delta H_c}{C_p T_\infty} Fr^{1/2} \quad Fr = \frac{u_{fuel}^2}{gd} \tag{42}$$

where ρ_{fuel}, u_{fuel}, ΔH_c, C_p are the density and injection velocity of the fuel, the heat of combustion and the specific heat; Fr is the Froude number.

On the basis of physical arguments, Regime 1 corresponds to $Q^\star \leq 1$ while Regime 2 corresponds to $Q^\star \geq 100$. Buoyant jet flames belong to the transition regime separating 1 and 2. Here, the values of $Q^\star$ are 0.19, 0.39, 0.77, 3.89 and 7.78 for the following heat release rates: 25, 50, 100, 500 and 1,000kW/m, respectively. The corresponding Froude numbers are $2.72\ 10^{-6}$, $1.08\ 10^{-5}$, 4.35

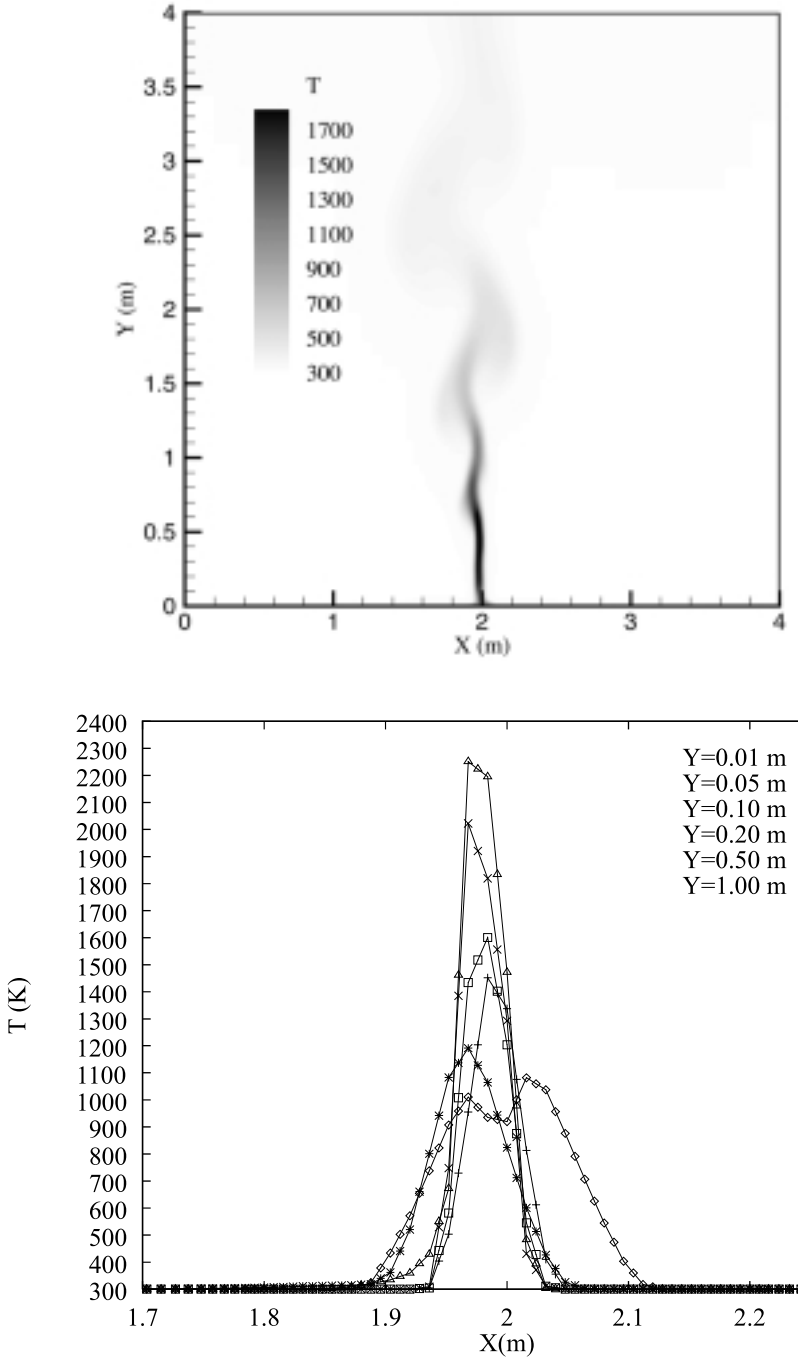

Figure 9.
Temperature field and temperature profiles obtained by neglecting radiation heat transfer for a 100kW/m methane/air flame

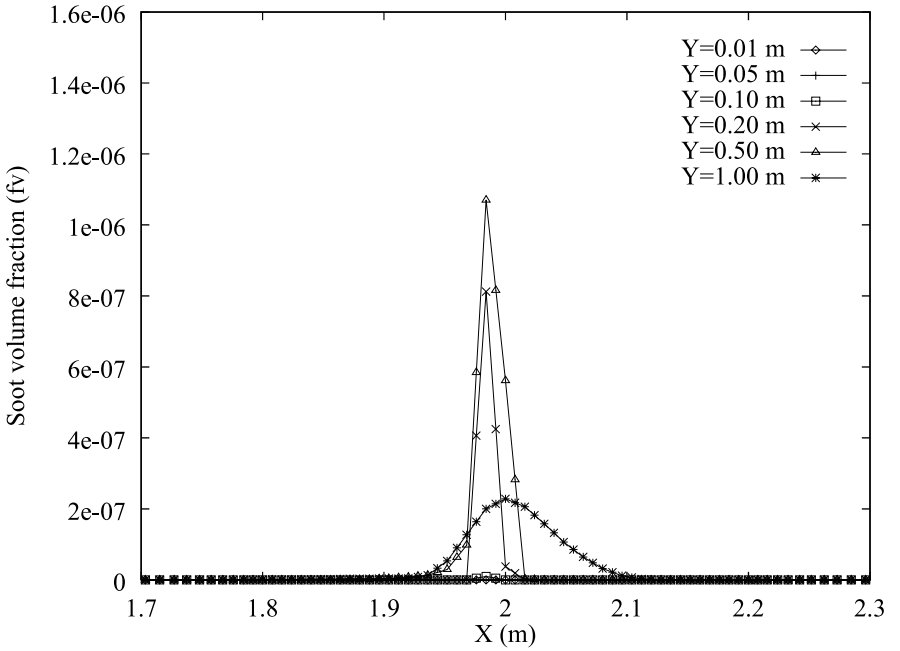

Figure 10.
Soot volume fraction profile at different heights (P = 100kW/m)

10^{-5}, 1.08 10^{-3} and 4.35 10^{-3}. According to the previous classification (Caffrey, 1988), the present calculations are typical of buoyant and jet flame regimes. Temperature and velocity vector fields observed for the buoyant flame regime (Figures 13 and 15) are characterized by large unsymmetrical coherent structures which develop alternatively on both sides of the hot gas above the flame. The corresponding thermal and hydrodynamic fields observed for the jet flame regime (Figures 14 and 16) are nearly symmetrical; the hot gas column above the flame is continuously accelerated along the thermal plume trajectory (from $\sim 1\mathrm{cm/s}$ at the burner to 9-10m/s near the flame tip). Figure 19 shows the time evolution of the stoichiometric flame height for the different heat release rates. It may be observed that for low values of P, the flame height becomes almost independent of the Froude number with a value of about 0.5m. A low-frequency behaviour (less than 1Hz) due to the development of large-scale Rayleigh-Taylor instabilities is characteristic of buoyancy-driven fires for which the hydrodynamic influence of fuel source momentum is small (Moss, 1995). For higher values of the Froude number, the flame height does not exhibit time oscillations and steady-state values of around 1.97 and 2.81m are obtained for $P = 500$ and P = 1,000kW/m respectively. These results are in agreement with a previous study which analyses the influence of the Froude number on the flame-vortex dynamic (Shu *et al.,* 1997). The distinction between regimes is clearly seen in Figures 17 and 18 where temperature profiles at different heights have been plotted. For heat release rate ranging from 25 to 100kW/m (Figures 7 and 17), the temperature profiles are quite sharp. A

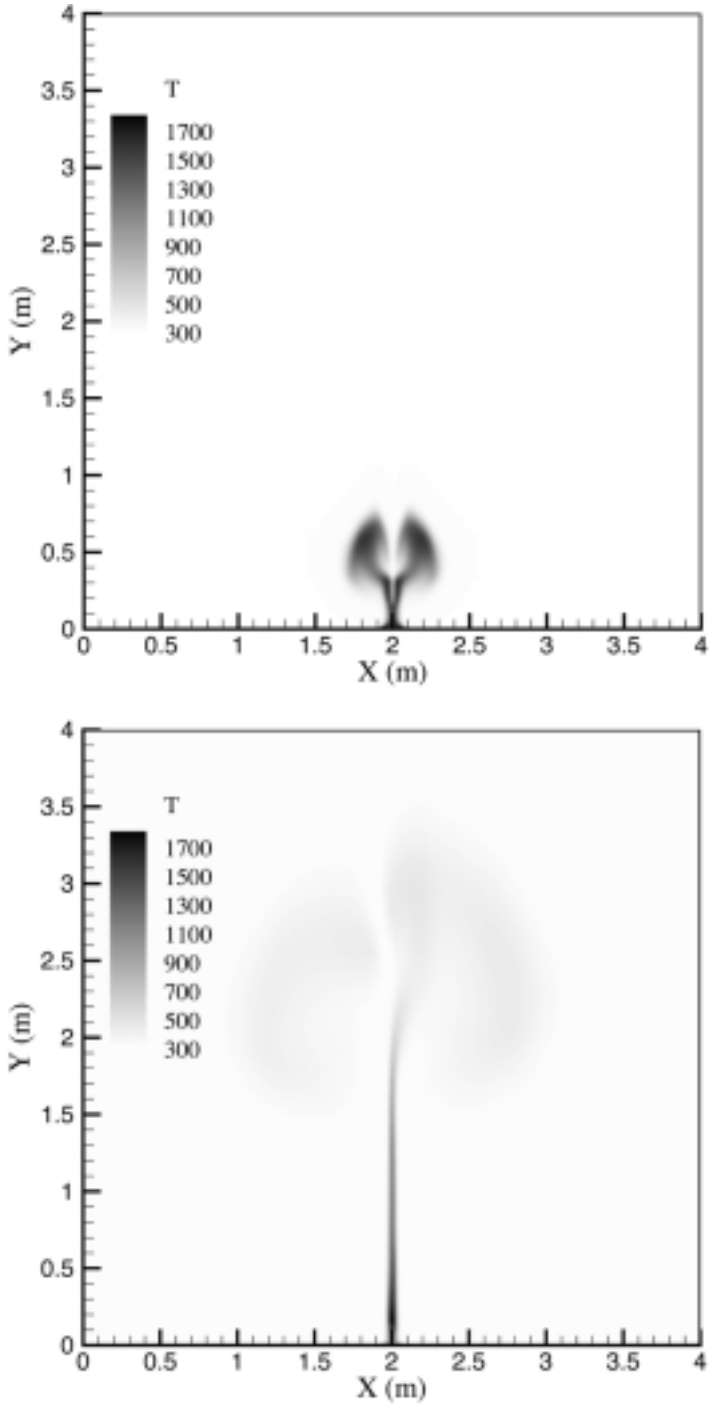

Figure 11.
Methane/air turbulent diffusion flame: temperature field obtained for heat release rate P = 100kW/m at time = 4s and 8s

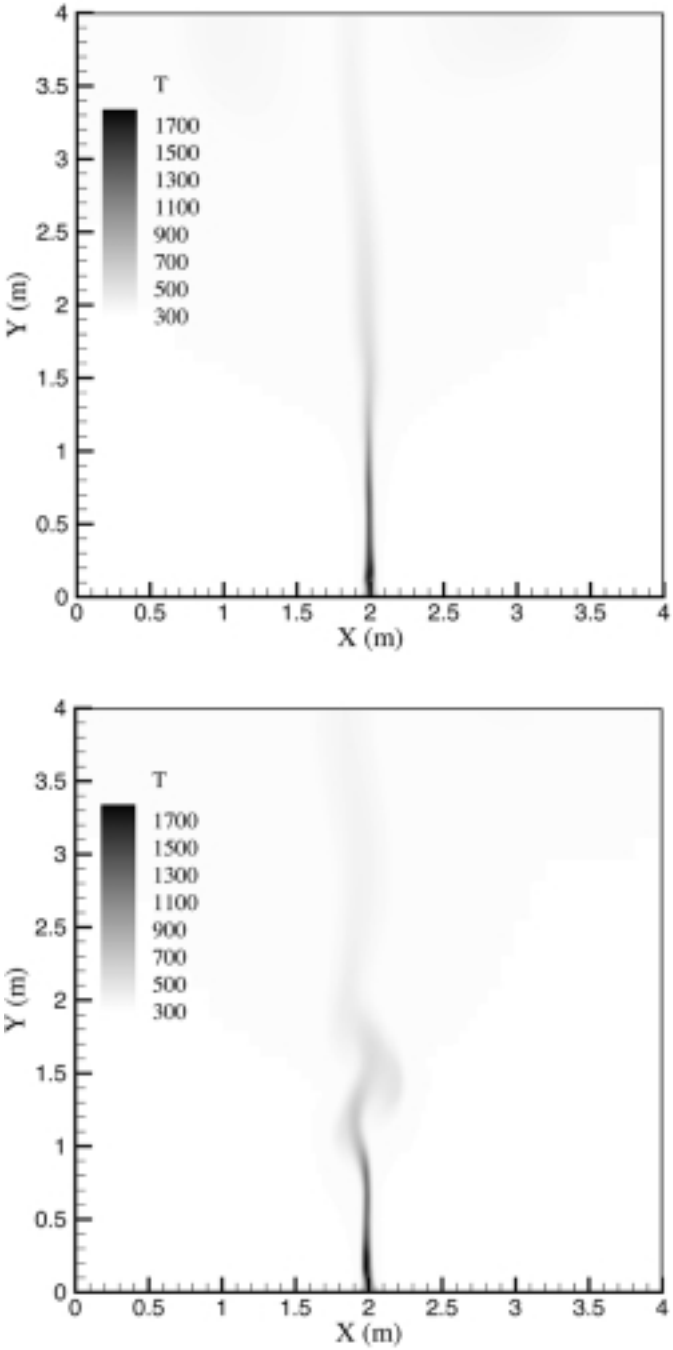

Figure 12.
Methane/air turbulent diffusion flame: temperature field obtained for heat release rate P = 100kW/m at time 12s and 16s

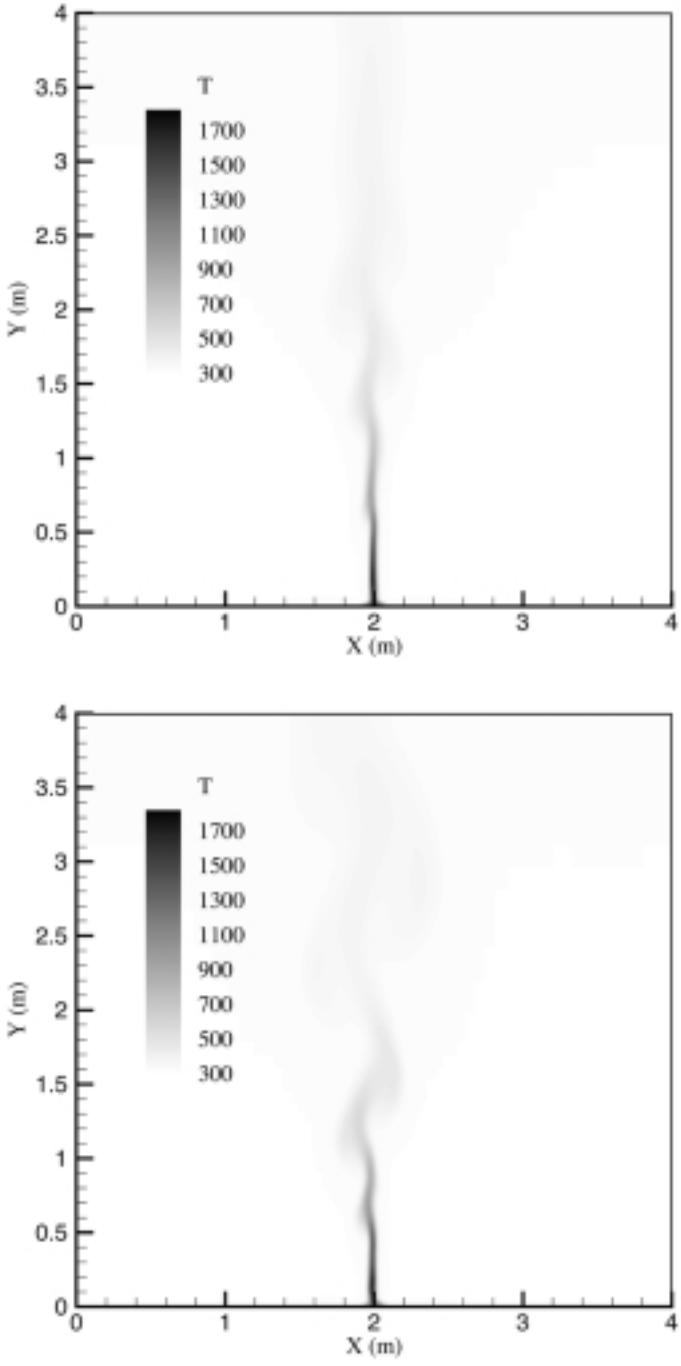

Figure 13.
Methane/air turbulent diffusion flame: temperature field obtained for heat release rates P =25 and 50kW/m

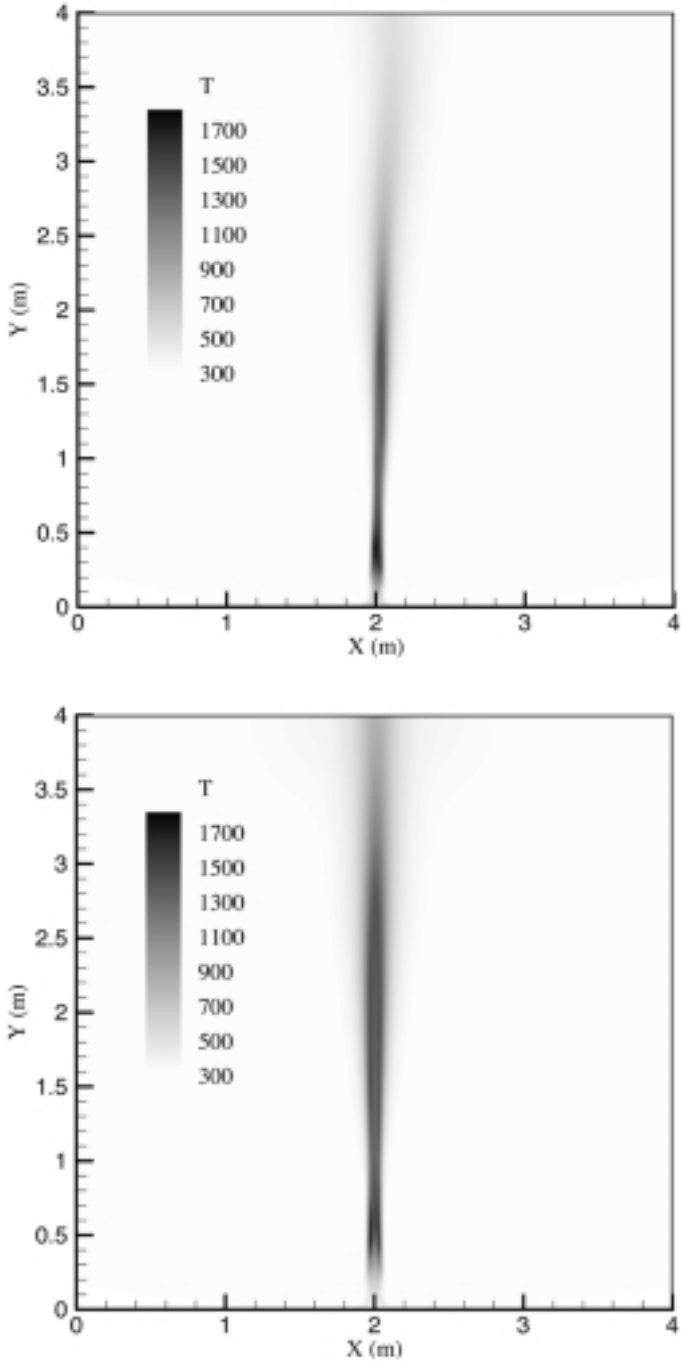

Figure 14.
Methane/air turbulent diffusion flame: temperature field obtained for heat release rates P = 500 and 1,000kW/m

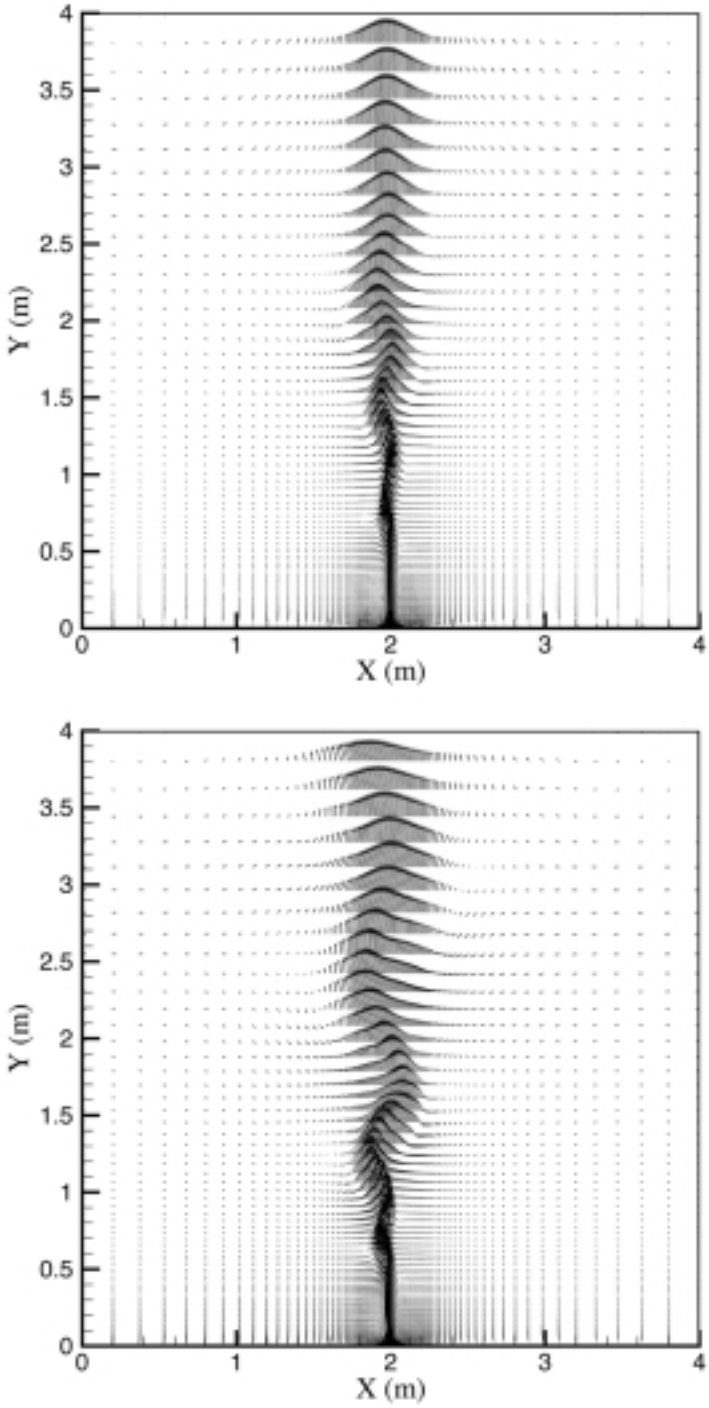

Figure 15.
Methane/air turbulent diffusion flame: velocity vectors field obtained for heat release rates P = 25 and 50kW/m (U_{max} = 4.7m/s)

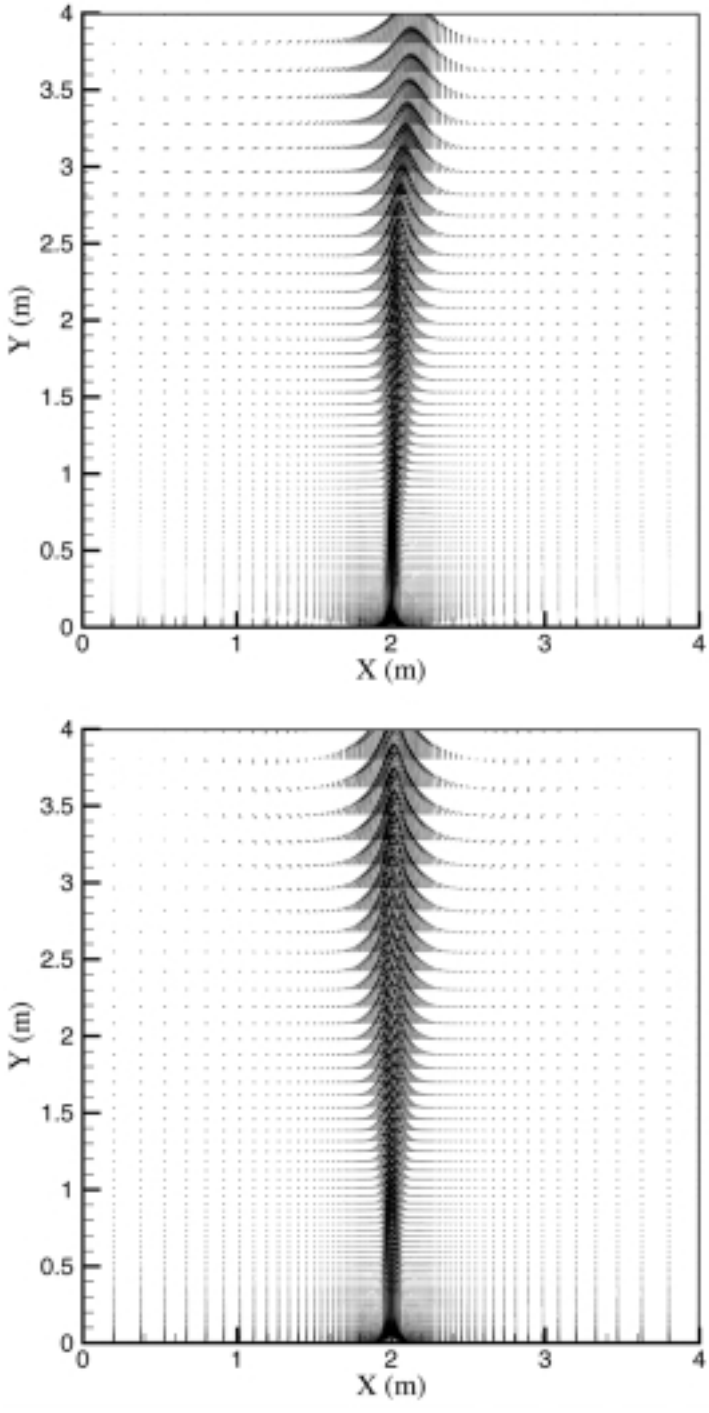

Figure 16.
Methane/air turbulent diffusion flame: velocity vectors field obtained for heat release rates P = 500 and 1,000kW/m (U_{max} = 8.1 and 10m/s, respectively)

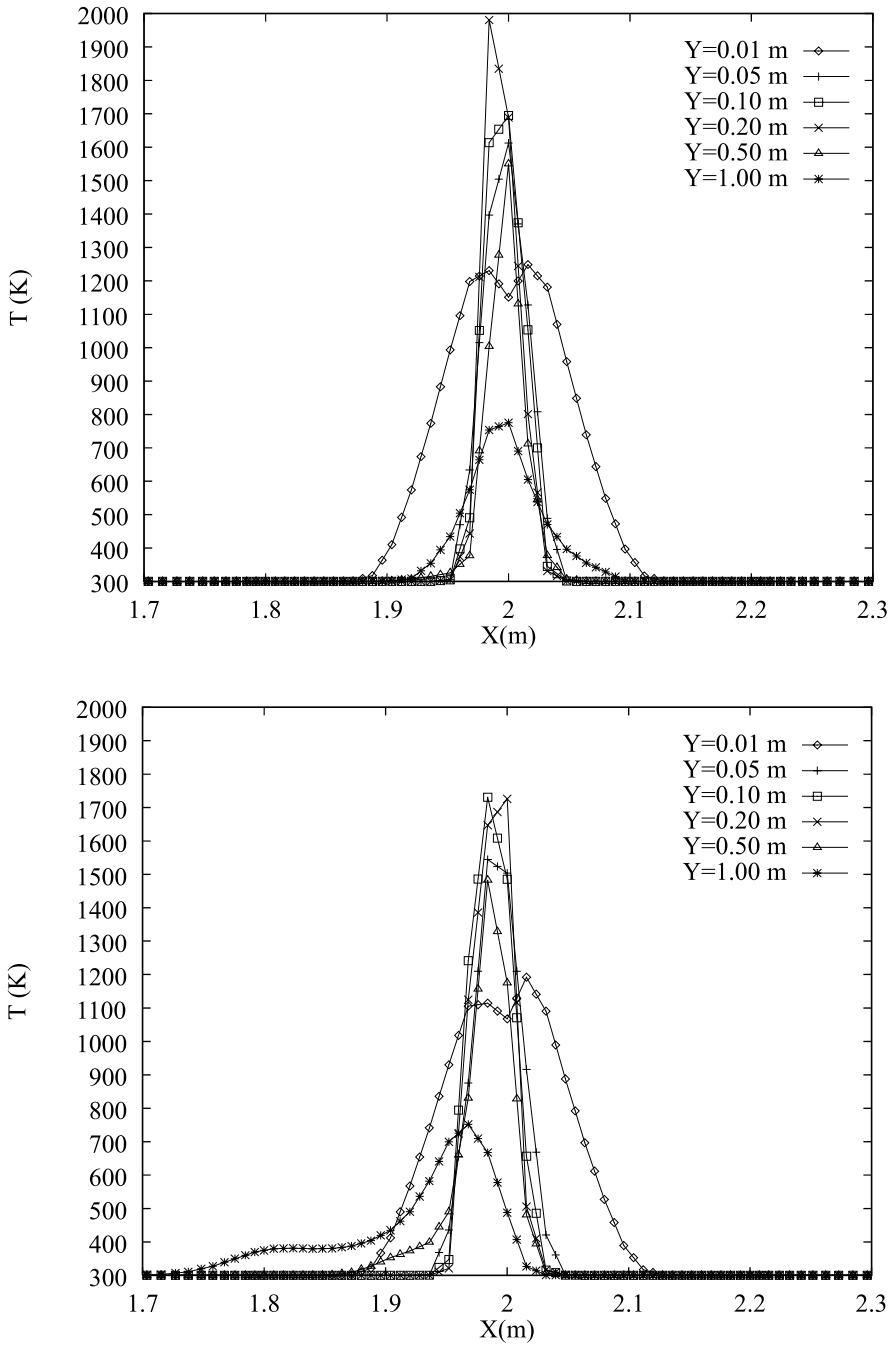

Figure 17.
Temperature profiles obtained for heat release rates P = 25 and 50kW/m

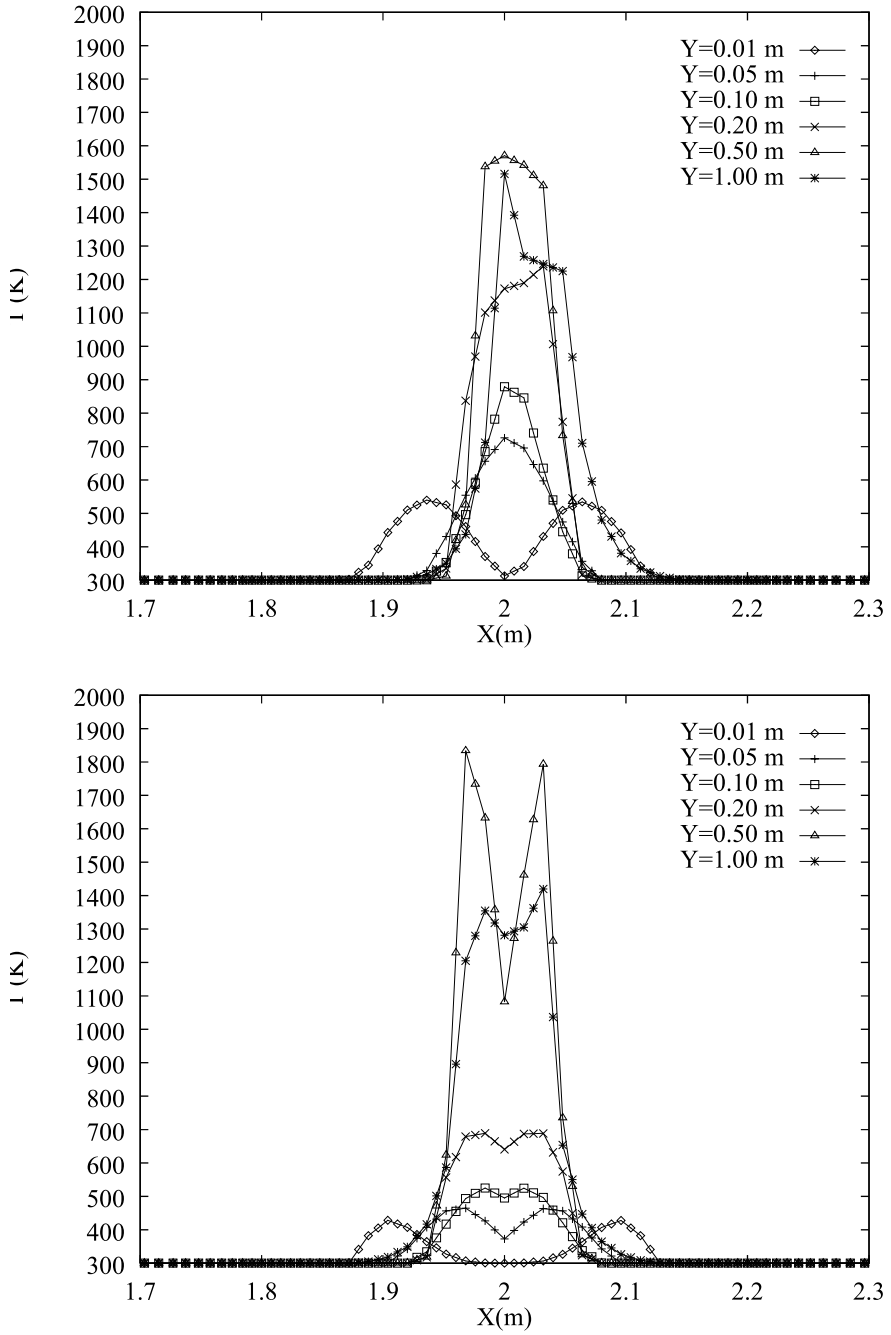

Figure 18.
Temperature profiles obtained for heat release rates P = 500 and 1,000kW/m

temperature maximum occurs at $0.1 \leq Y \leq 0.2\mathrm{m}$. Also shown is the hot gas core at about 1,100-1,200K at $Y = 0.01\mathrm{m}$ which represents the pre-flame zone. At higher rates, a widening of the thermal plume is observed and the temperature maximum appears at 0.5m. Unlike Regime 1, near the burner exit, at $Y = 0.01\mathrm{m}$, the temperature profile is composed of a cold gas core ($T \sim 300K$) bounded by two temperature peaks at the stoichiometric flame location. By increasing the fuel injection rate, the volume of the fuel-rich region near the burner is increased. In Figures 20 and 21 soot volume fraction fields and profiles at different heights for the extreme cases of $P = 25$ and 1,000kW/m are presented. Because the production source terms in the soot transport equation are temperature dependent, soot production occurs in the hot gas region and a maximum in soot volume fraction appears at $Y = 0.5m$ for a low heat release rate ($P = 25\mathrm{kW/m}$) and at $Y = 1.0\mathrm{m}$ for a higher value ($P = 11{,}000\mathrm{kW/m}$), respectively $6\,10^{-7}$ and $1.5\,10^{-6}$.

5. Conclusions

The behaviour of a turbulent diffusion flame has been studied numerically using a high order finite volume method. The resolution is performed using a VLES approach combining RNG unsteady k-ϵ turbulence modelling and the use of eddy dissipation concept for the evaluation of the reaction rate. The radiative heat transfer induced by soot production in the flaming zone has been taken into account in the energy balance inside the gas mixture. Numerical results show that the energy lost by radiation in the gas can represent $\sim$ 20-25 percent

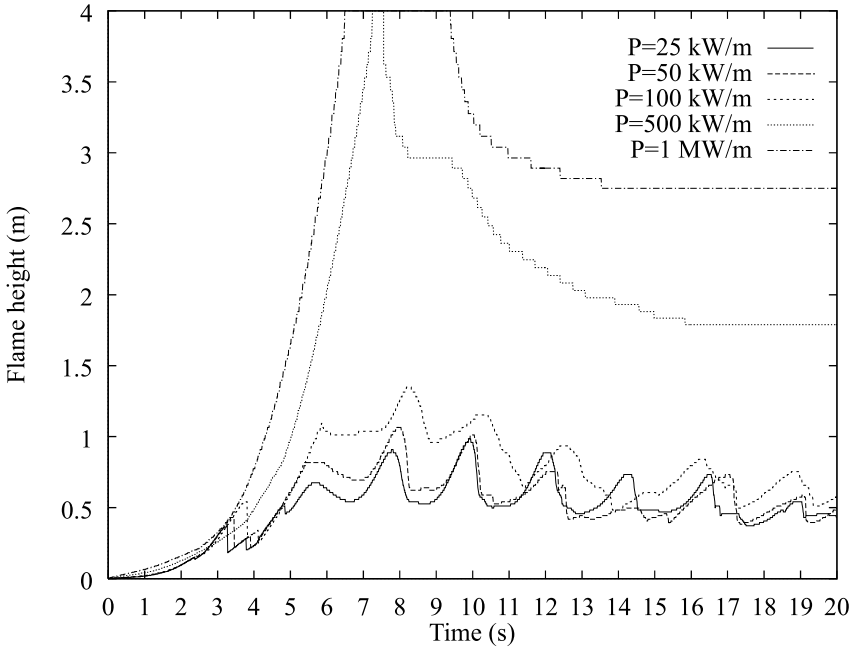

Figure 19.
Time evolution of the flame height for different heat release rates

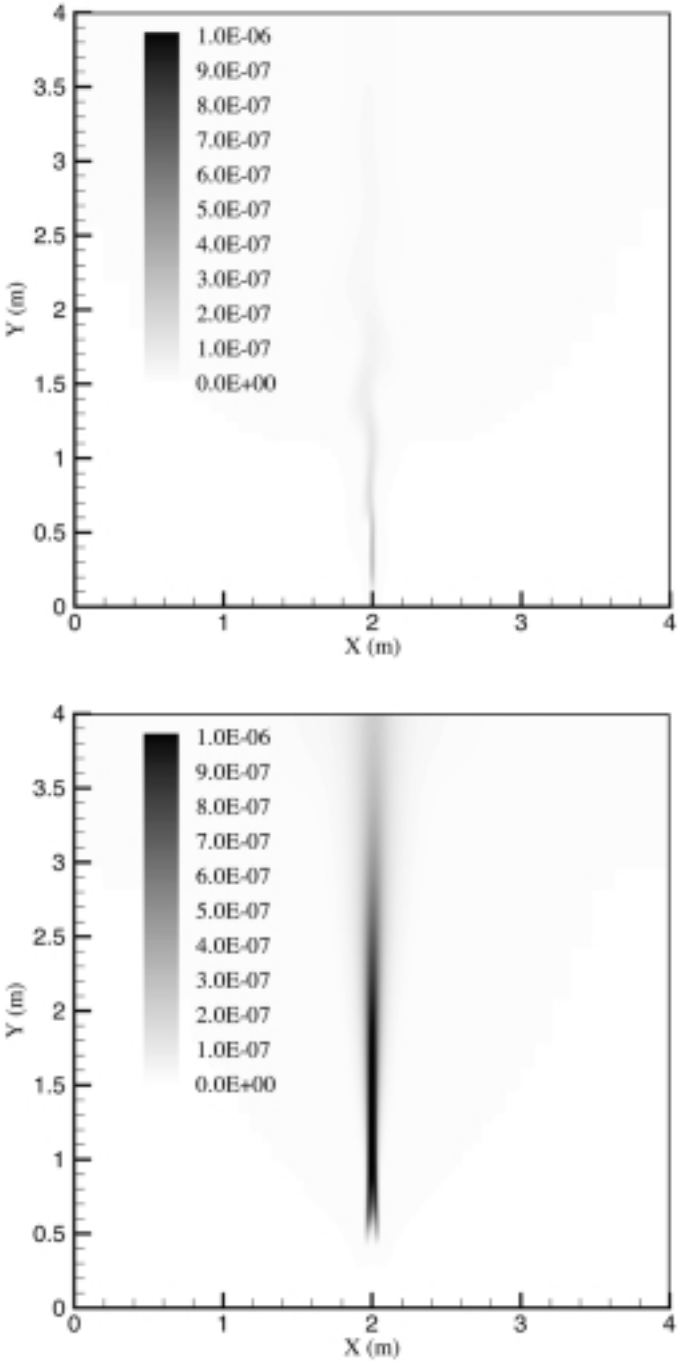

Figure 20.
Soot volume fraction field obtained for heat release rates $P = 25$ (top) and 1,000kW/m (bottom)

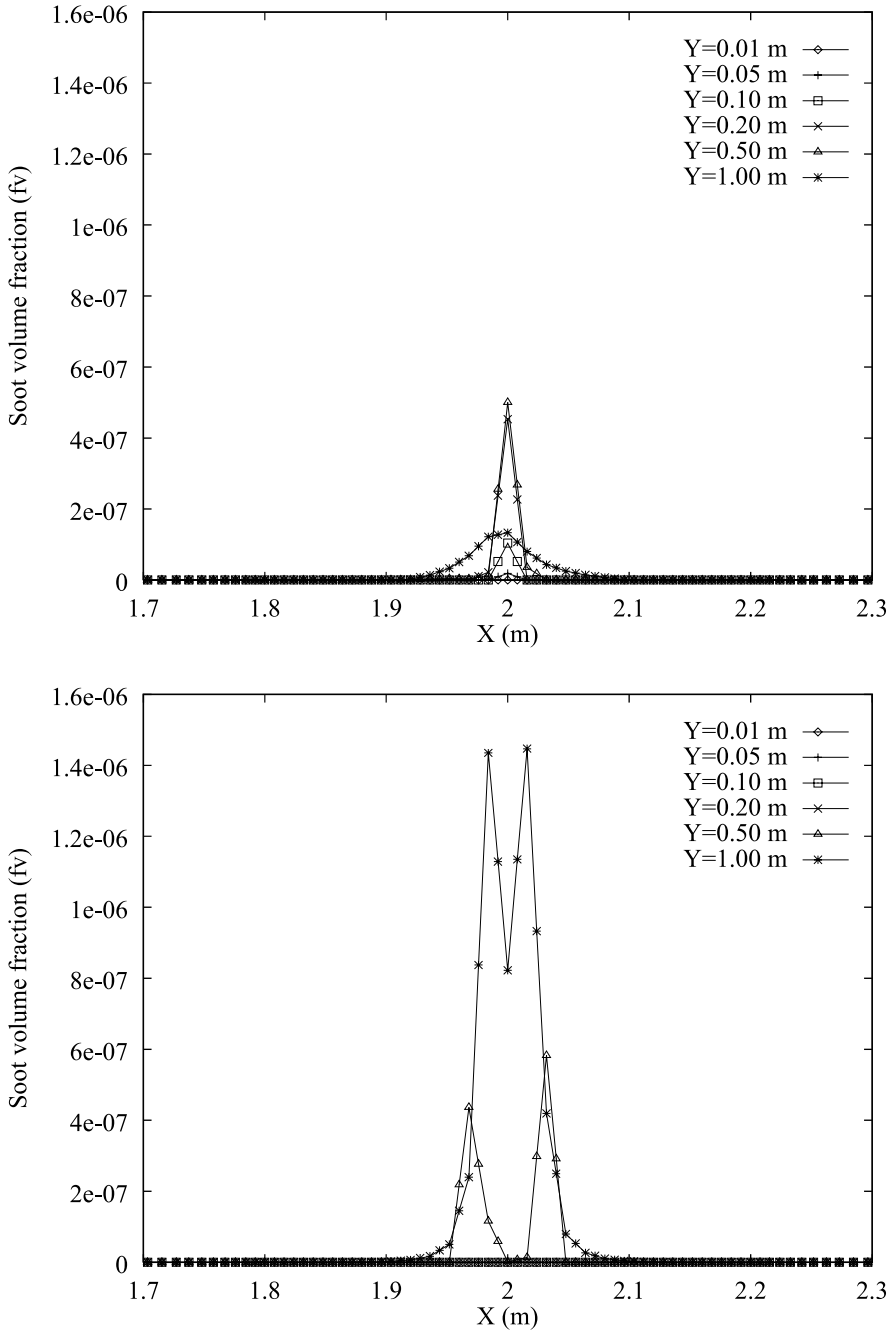

Figure 21.
Soot volume fraction profiles obtained for heat release rates $P = 25$ (top) and 1,000kW/m (bottom)

of the heat released by the combustion reaction. For small Froude numbers, the buoyant flow above the flame exhibits an unsteady behaviour with large scale structures due to the development of both buoyancy-driven and shear-layer instabilities. At high Froude numbers, results indicate the absence of a significant rollup process, with the flame exhibiting a steady-state and symmetrical structure.

References

Borghi, R. (1988), "Turbulent combustion modelling", *Prof. Energy Combust. Sci.*, Vol. 14, pp. 245-92.

Bray, K. (1996), "The challenge of turbulent combustion", *26th Symposium. (International) on Combustion, The Combustion Institute*, pp. 1-26.

Caffrey, M. (1988), *Flame Height*, National Fire Protection Association, Quincy, MA, pp. 1-18.

Candel, S., Thevenin, D., Darabiha, N. and Veynante, D. (1996), "Problems and perspectives in numerical combustion", *Computational Methods in Applied Sciences, Eccomas 96*, pp. 48-62.

Cox, G. (1995), *Combustion Fundamentals of Fire*, Academic Press, New York, NY.

Davis, R., Moore, E. and Roquemore, W. (1991), "Preliminary results of a numerical-experimental study of the dynamic structure of a buoyant jet diffusion flame", *Combust. Flame*, Vol. 83, pp. 262-70.

Drysdale, D. (1985), *An Introduction to Fire Dynamics*, John Wiley and Sons, New York, NY.

Fusegi, T. and Farouk, B. (1989), "Laminar and turbulent convection-radiation interactions in a square enclosure filled with a non-grey gas", *Numerical Heat Transfer, Part A*, Vol. 15, pp. 303-22.

Gatski, T., Hussaini, M. and Lumley, J. (1996), *Simulation and Modeling of Turbulent Flows*, Oxford, University Press, Oxford.

Jones, W. and Whitelaw, J. (1983), "Calculation methods for reacting turbulent flows: a review", *Combust. Flame*, Vol. 48, pp. 1-26.

Kaplan, C., Shaddix, C. and Smyth, K. (1996), "Computations of enhanced soot production in time-varying ch_4/*air* diffusion flames", *Combust. Flame*, Vol. 106, pp. 393-405.

Kaplan, C., Baek, S., Oran, E. and Ellzey, J. (1994), "Dynamics of a strongly radiating unsteady ethylene jet diffusion flame", *Combust. Flame*, Vol. 96, pp. 1-21.

Leonard, B. and Drummond, J. (1995), "Why you should not use hybrid, power-law or related exponential schemes for convection modelling – there are much better alternatives", *Int. J. Numerical Methods*, Vol. 20, pp. 421-42.

Leonard, B. and Mokhtari, S. (1990), "Beyond first-order upwinding: the ultra-sharp alternative for non-oscillatory steady-state simulation of convection", *Int. J. Numerical Methods Engineering*, Vol. 30, pp. 729-66.

Libby, P. and Williams, F. (1993), *Turbulent Reacting Flows*, Academic Press, New York, NY.

Magnussen, B. and Hjertager, H. (1976), "On mathematical modeling of turbulent combustion with special emphasis on soot formation and combustion", *Proceeding of 16th Symposium (International) on Combustion, The Combustion Institute*, pp. 719-29.

Mohammadi, B. and Pironneau, O. (1994), *Analysis of the K-Epsilon Turbulence Model*, John Wiley and Sons, Masson.

Moss, J. (1995), Cox, G. (Ed.), *Turbulent Diffusion Flames*, Academic Press, New York, NY, pp. 221-72.

Orszag, S. (1996), *Introduction to Renormalization Group Modeling of Turbulence*, Oxford University Press, Oxford, pp. 155-83.

Patankar, S. (1981), "A calculation procedure for two-dimensional elliptic situations", *Numerical Heat Transfer*, Vol. 4, pp. 409-25.

Said, R., Garo, A. and Borghi, R. (1997), "Soot formation modeling for turbulent flames", *Combust. Flame*, Vol. 108, pp. 71-86.

Schiestel, R. (1993), *Modelisation et simulation des ecoulements turbulents*, Hermes.

Shu, Z., Aggarwal, S., Katta, V. and Puri, I. (1997), "Flame-vortex dynamics in an inverse partially premixed combustor: the Froude number effects", *Combust. Flame*, Vol. 11, pp. 276-95.

Siegel, R. and Howell, R. (1992), *Thermal Radiation Heat Transfer*, Hemisphere, Washington, DC.

Speziale, C. (1987), "On non-linear k-1 and k-ε models of turbulence", *J. Fluid Mech.*, Vol. 178, pp. 459-75.

Yakhot, V. and Orszag, S. (1986), "Renormalization group analysis of turbulence", *J. Scientific Computing*, Vol. 1 No. 1, pp. 3-51.

Yakhot, V. and Smith, M. (1992), "The renormalization group, the ε-expension and derivation of turbulence models, *J. Scientific Computing*, Vol. 7 No. 1, pp. 35-61.

Zijlema, M., Segal, A. and Wesseling, P. (1995), "Finite volume computation of incompressible turbulent flows in general co-ordinates on staggered grids", *Int. J. Numerical Methods Fluids*, Vol. 20, pp. 621-40.